PCCP

Cite this: *Phys. Chem. Chem. Phys.*, 2012, **14**, 4817–4823

www.rsc.org/pccp

PAPER

Evanescent photosynthesis: exciting cyanobacteria in a surface-confined light field†

Matthew D. Ooms,[a] Vincent J. Sieben,[b] Scott C. Pierobon,[a] Erica E. Jung,[c] Michael Kalontarov,[c] David Erickson[c] and David Sinton*[a]

Received 27th January 2012, Accepted 15th February 2012
DOI: 10.1039/c2cp40271h

The conversion of solar energy to chemical energy useful for maintaining cellular function in photosynthetic algae and cyanobacteria relies critically on light delivery to the microorganisms. Conventional direct irradiation of a bulk suspension leads to non-uniform light distribution within a strongly absorbing culture, and related inefficiencies. The study of small colonies of cells in controlled microenvironments would benefit from control over wavelength, intensity, and location of light energy on the scale of the microorganism. Here we demonstrate that the evanescent light field, confined near the surface of a waveguide, can be used to direct light into cyanobacteria and successfully drive photosynthesis. The method is enabled by the synergy between the penetration depth of the evanescent field and the size of the photosynthetic bacterium, both on the order of micrometres. Wild type *Synechococcus elongatus* (ATCC 33912) cells are exposed to evanescent light generated through total internal reflection of red (λ = 633 nm) light on a prism surface. Growth onset is consistently observed at intensity levels of 79 ± 10 W m^{-2}, as measured 1 μm from the surface, and 60 ± 8 W m^{-2} as measured by a 5 μm depthwise average. These threshold values agree well with control experiments and literature values based on direct irradiation with daylight. In contrast, negligible growth is observed with evanescent light penetration depths less than the minor dimension of the rod-like bacterium (achieved at larger light incident angles). Collectively these results indicate that evanescent light waves can be used to tailor and direct light into cyanobacteria, driving photosynthesis.

1. Introduction

Since prehistoric times, photosynthetic microorganisms have played an essential role in the carbon cycle and as the primary mechanism for solar energy capture[1] in the biosphere. In modern times, their demonstrated performance has resulted in significant interest from industry and research for the potential uses of photosynthetic microorganisms in such diverse areas as bioremediation,[2] pharmaceuticals,[3] human health,[4] and biofuel production.[5–7] Furthermore, the photosynthetic machinery of these organisms has provided clues leading to the development of improved photoelectrochemical conversion and energy capture devices.[8] These photosynthetic microorganisms, which include a variety of bacteria species and green algae, have varied nutritional requirements but all rely on absorption of light to fuel their metabolic processes. Illuminating cells in confined environments, at high density, and with the control required by precise laboratory studies can present challenges, particularly when scales approach those of the organisms themselves.

Current methods of delivering light energy to microorganisms vary depending on scale, but generally rely on bulk illumination of suspended cultures.[5] Large scale production photobioreactors rely on direct solar illumination in either racetrack style, open air ponds[9] or fully enclosed transparent structures[10,11] to provide the necessary energy for photosynthesis. Solar radiation may be complimented or replaced by artificial light sources, particularly in research laboratory applications, in order to achieve more controlled lighting conditions.[12–14] Improved spatial dilution of light within the culture volume has been achieved through the addition of light-guiding elements[15–18] that help scatter light into darker regions of high density cultures. Microfluidic systems have also been identified as attractive platforms on which to study cell cultures on the cellular scale and offer advantages over larger scale devices when it comes to studying the growth

[a] *Department of Mechanical and Industrial Engineering, University of Toronto, Toronto, ON, Canada M5S 1A1. E-mail: sinton@mie.utoronto.ca; Fax: +1-416-978-7753; Tel: +1-416-978-1623*
[b] *Department of Mechanical Engineering, University of Victoria, Victoria, BC, Canada V8P 5C2*
[c] *Sibley School of Mechanical and Aerospace Engineering, Cornell University, Ithaca, NY, USA 14853. E-mail: de54@cornell.edu; Fax: +1-607-255-1222; Tel: +1-607-255-4861*
† Electronic supplementary information (ESI) available. See DOI: 10.1039/c2cp40271h

dynamics and behaviour of the organisms.[19–23] All large and small scale cultivation systems developed to date, however, rely on radiant bulk illumination. An illumination strategy that confines and delivers light on the scale of the microorganism would enable improved control and quantification.

In this paper we demonstrate the excitation of photosynthetic cyanobacteria using the evanescent light field confined to the surface of a waveguide. The method we describe is enabled by the synergy between the fundamental penetration depth of the evanescent field and the size of the photosynthetic microorganism, both on the order of micrometres. Evanescent coupling is demonstrated using a circular cross-section laser beam incident on the surface of a prism at an angle greater than critical such that the beam undergoes total internal reflection. This setup generates an elliptical evanescent field profile on the prism surface. The resulting field decays exponentially into the medium and is confined only to a narrow region above the prism. *Synechococcus elongatus* (ATCC 33912) is shown to grow preferentially in this field in a manner that is related to optimal radiant light levels for these bacteria. This work provides an alternative to current practices of delivering radiant light to cultures of photosynthetic bacteria by providing a means to confine and control the delivery of energy on the cellular scale.

2. Method and materials

2.1 Bacteria cultures

In all experiments, cells of the wild type *S. elongatus* (ATCC 33912) cyanobacteria were used. Culture growth rate is strongly dependent on fluid temperature and irradiation intensity.[24] Cells were cultured under optimal conditions of 32–36 °C and under continuous irradiation of 50–75 μE m^{-2} s^{-1} using fluorescent lamps, as described previously.[24–26] The stock culture was kept at a constant cell density (in the exponential growth phase), by regularly diluting the culture with fresh BG11 cyanobacteria growth medium (Sigma Aldrich C3061) to maintain a constant optical density of 0.2 at 750 nm (OD_{750}). The OD_{750} was determined using a broad spectrum halogen light source (Thorlabs OSL1) and a spectrometer (Edmond brc112e) and normalized to the OD_{750} of fresh BG11 growth media. Samples of this culture were used for all experiments.

2.2 Experimental apparatus

Cavities to contain the bacteria culture solution were fabricated by moulding PDMS (Sylgard(R) 184 Elastomer Kit, Dow Corning) around a poly(methylmethacrylate) (PMMA) master to create cylindrical cavities 10 mm in diameter and 5 mm deep (0.4 mL). These culture cavities were bonded to the surface of 1 mm thick BK7 glass microscope slide using oxygen plasma treatment.[27]

Once mounted to the glass plates and inoculated (dead end filling *via* syringe injection), the cultures were placed on the top faces of right angle BK7 prisms (Thorlabs PS908L-A), as shown in Fig. 1, and the cells were allowed to settle onto the surface of the glass slide. Optical contact was achieved using an index matched immersion oil (Leica 11513 859). Light was coupled to the chamber from a helium neon laser (633 nm Thorlabs HRR020) directed toward the prism by reflecting it

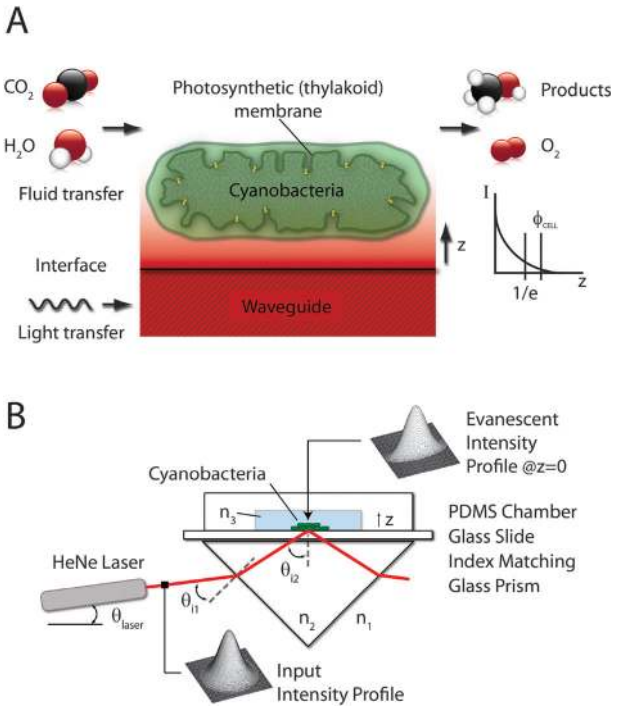

Fig. 1 Exciting photosynthetic bacteria with the evanescent light field. (A) Schematic showing evanescent coupling of a photosynthetic bacterium on the surface of a waveguide. The characteristic decay of the red light intensity, as plotted at right, is on the order of the cell size. (B) Experimental setup to generate the evanescent wave at the surface of the glass slide. The input beam is Gaussian and the evanescent field resulting from total internal reflection is elliptical in shape, as shown.

off a broadband dielectric mirror (Thorlabs CM1-4E) mounted to a precision rotation mount (Thorlabs CRM1P). The incident angle at the glass media interface was adjusted by changing the angle of the mirror in the rotation mount. The prism/culture assembly was mounted to a sliding stage, which allowed the laser beam to be maintained in the centre of the culture chamber as the angle of incidence was varied. The prism assembly was aligned such that the reflection of the beam leaving the prism did not pass through the culture. This ensured that optical excitation of the bacteria was solely due to the evanescent field where the beam was totally internally reflected at the glass–bacteria culture interface.

Laser beam power into and out of the prism was measured using a photodiode power sensor (Thorlabs S120C) and measured once at the beginning of the experiment and once at the end. The entire experimental apparatus was optically isolated in enclosures made from 5 mm thick hardboard (Thorlabs TB4). These chambers were kept at a constant temperature of 32–36 °C for optimal cell growth rates for the duration of the evanescent growth experiments using a 950 W enclosure fan heater (CR030599, OMEGA Engineering Inc., USA).

2.3 Measurement of growth rings

Growth patterns were imaged using standard bright field microscopy techniques. Images were collected using an SLR camera (Nikon D60) fitted to an upright microscope (Leica DMLM/P).

The images were captured at 5× magnification using identical camera settings (exposure, colour parameters, *etc*.). Multiple images were required to capture the full spatial extent of the growth rings at this magnification. The individual images were then compiled in an automated fashion to create a composite image of each growth ring. The composites were then processed in Matlab employing colour thresholding to identify pixels with Green/Red and Green/Blue ratios larger than 1. A normalized histogram was created for pixels that satisfied these criteria, based on their radial distance from the centre of the beam profile (the elliptical profiles were converted to circular profiles using the experimental angles and Snell's law).

3. Results and discussion

The evanescent excitation approach is shown in Fig. 1A. A bacterium on the surface of the waveguide receives light from the evanescent light field which decays rapidly with distance from the surface. The prism-based experimental setup used to generate the evanescent field is shown in Fig. 1B. The evanescent field develops at the interface between the liquid and the glass where the light is totally internally reflected.[28,29] Total internal reflection and the corresponding evanescent field result when light is incident at the glass–media interface at angles greater than the critical angle, $\theta_{i2} > \theta_C$. Reflecting a circular cross-section input beam develops an elliptical evanescent field at the point of reflection, as shown. While there are many ways to generate an evanescent field, this approach is simple and importantly provides an evanescent light field distribution that can be reliably described with theory in all three dimensions.

Cell cultures were first placed under direct laser light exposure, to establish the effectiveness of using monochromatic red (λ = 633 nm) at growing *S. elongatus*, and measure cell response to direct radiation light. The beam from a Helium–Neon (HeNe) laser was passed through a culture cavity perpendicular to the bottom glass slide and the culture was left to grow for 72 hours (under conditions described in the Method and materials section). This type of direct irradiation experiment was done for various laser powers, yielding consistent results to those shown in Fig. 2. Fig. 2A shows a typical growth ring pattern, where the effect on growth from the three distinct intensity regions is evident. There is a bleached (yellowish orange) region in the centre, a growth region (green) and a negligible-growth outer region. To quantify growth in a radial profile, the image was filtered for green intensity and integrated in circumference (details in Method and materials). The resulting radial growth profile is plotted with the laser intensity profile in Fig. 2B. The threshold electric field intensities (low and high) between regions were determined from the intersection of the full width at half maximum (FWHM) growth locations and the incident light power profile. The resulting threshold values of 66 W m^{-2} and 12 W m^{-2} (shown in Fig. 2B by the rectangle within the growth peak) indicate the productive growth intensities of *S. elongatus* under direct irradiation at λ = 633 nm.

Relating these direct irradiation experiment results to known growth characteristics of *S. elongatus* requires estimating the daylight equivalent power of red light at λ = 633 nm. To do so, we compared radiometric measurements of daylight to optimal intensity ranges published in the literature. At high light

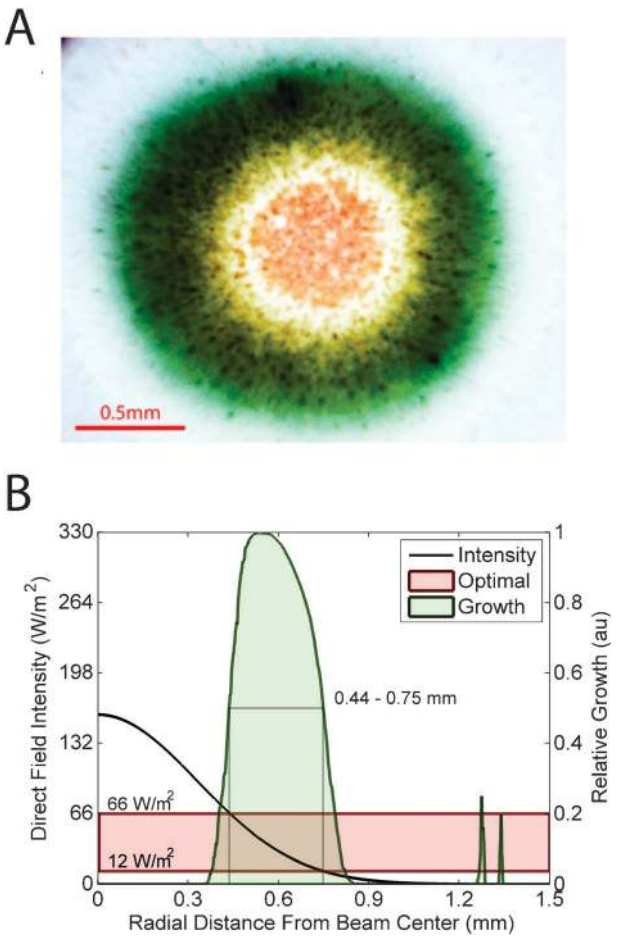

Fig. 2 Growing photosynthetic bacteria using *direct* irradiation. (A) Image of cyanobacteria growth pattern resulting from direct irradiation, showing distinct regions of photobleaching (centre), growth, surrounded by negligible growth. (B) Plot correlating radial growth intensity to laser light intensity. Outlying peaks beyond 1.2 mm are artefacts of the imaging setup and do not correspond to growth. FWHM thresholds on the growth region correspond to radiant light intensities of 66 W m^{-2} and 12 W m^{-2}, shown as upper and lower bounds, respectively.

intensities, the rate of radiation induced damage to the cell's photosystems exceeds the cell's ability to repair itself and the result is a sharp decrease in photosynthetic activity, or photoinhibition.[31] Photoinhibition can further lead to excessive destruction of light absorbing pigments, primarily chlorophyll a within the cell's photocenters, in a process known as photobleaching.[32] High light conditions that approach saturating intensities are reported as a Photosynthetic Photon Flux Density (PPFD) on the order of 150 μE m^{-2} s^{-1} to 500 μE m^{-2} s^{-1} in the Photosynthetically Active Radiation (PAR) wavelength range (400–700 nm), or 10–25% of full daylight.[31,33–35] To convert the photosynthetic photon flux density to radiometric units (*i.e*. W m^{-2}), the optical power of full daylight was measured at 635 nm to be 1.37 W m^{-2} (48°25′43″N 123°21′56″W). The spectral power distribution of normal daylight was then calculated from this set point and the relative spectral power distribution defined by CIE Standard Illuminant D65,[30] as shown in Fig. 3. Total full

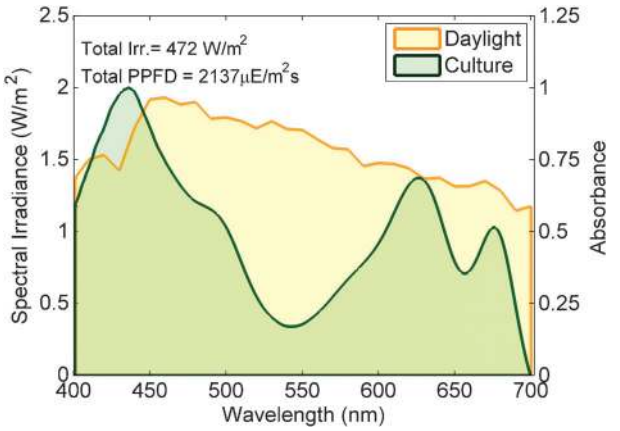

Fig. 3 Spectral power distribution of daylight[30] and normalised absorption spectrum of *S. elongatus* culture. The photoinhibition threshold at $\lambda = 633$ nm measured from experiments in Fig. 2 (66 W m^{-2}) correlates to established photoinhibition intensities of white light exposure, when related through the absorption spectrum shown.

daylight irradiance of photosynthetically active radiation was calculated to be 472 W m^{-2}, which corresponds to a photosynthetic photon flux density of 2137 μE m^{-2} s^{-1}. This value was independently confirmed by a QSR-2100 (Biospherical Instruments Inc.) light meter measurement of 2100–2300 μE m^{-2} s^{-1}. Also shown in Fig. 3 is the absorption spectrum for the cell cultures used for these experiments. Absorption peaks at $\lambda = 435$ nm, $\lambda = 625$ nm, and $\lambda = 677$ nm are typical for *S. elongatus*[36] and represent absorption by the light harvesting pigments Chl a ($\lambda = 435$ nm and $\lambda = 677$ nm) and the phycobilisomes of the photosystem II antenna structures—primarily phycocyanin (625 nm).[36]

Under normal daylight conditions, the effective photon flux seen by *S. elongatus* given its varied absorption ability for different wavelengths of light is 1044 μE m^{-2} s^{-1} of photosynthetically active radiation (400 nm $< \lambda <$ 700 nm). This is determined by weighing the spectral power distribution for daylight by the normalized absorption spectrum of the cell culture and integrating across the photosynthetically active region. It should be noted that this value represents a best case maximum for absorbed photosynthetic energy and assumes that all energy absorbed by the bacteria is funnelled into the photosynthetic infrastructure of the cell. To determine a corresponding irradiance for monochromatic light at $\lambda = 633$ nm that would simulate these daylight conditions, this broad-spectrum photon flux is multiplied by the energy contained in 1 μE of photons with $\lambda = 633$ nm (*i.e.* 0.189 J μE^{-1} determined from the Planck–Einstein equation) and divided by the normalized absorption of the cell culture at 633 nm (*i.e.* 0.65). This results in an irradiance of 301 W m^{-2} of $\lambda = 633$ nm light that is required to simulate the photosynthetic photon flux of normal daylight. Since the threshold for the onset of photobleaching measured in the direct irradiation experiments was 66 W m^{-2}, it can be inferred that ~22% of full daylight is the upper limit for our cultures before severe photobleaching occurs. This value agrees well with the upper bounds of what are considered high-light conditions in the literature.[31,33–35] Two key assumptions made here are that (1) photons of all energies within the photosynthetically active region have an equal potential to contribute to photobleaching and (2) the absorption of light by the cell is primarily due to pigments associated with light harvesting and energy transfer to the photosynthetic reaction centers. Given that the quantum efficiency of photosynthesis is known to be high[37] and that the daylight equivalent power for red light calculated here agrees generally with the onset of photobleaching both under red light conditions determined experimentally in this study and those under daylight conditions published in the literature,[31,33–35] these assumptions are considered justified for an order of magnitude estimate.

The light intensity distribution in an evanescent light field varies both in the plane of the surface and depthwise into the media. Established theory was applied to describe the evanescent electric field intensity and used to correlate field strength to experimental growth results (model details in ESI†). Fig. 4A shows the penetration depth of the evanescent light field as a function of incident angle. Here, the penetration depth is quantified as the location where the field intensity drops e^{-2}, or 87%, of the peak intensity at the surface. The geometry of *S. elongatus* is shown in the inset of Fig. 4A for reference, and

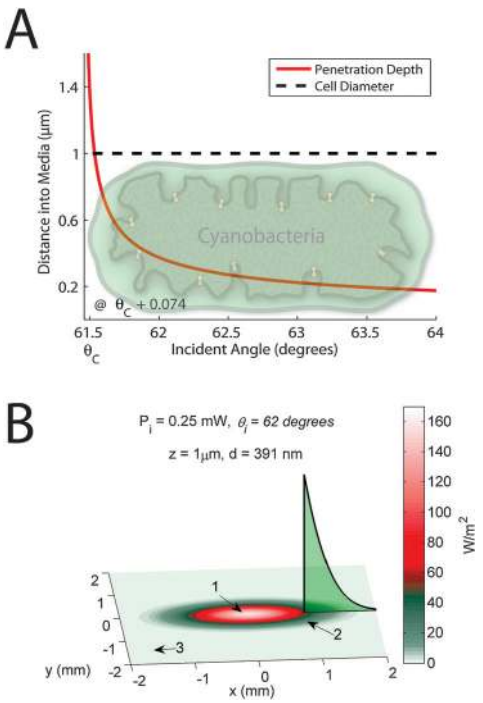

Fig. 4 Theoretical light intensity distribution in the evanescent light field, and corresponding predicted growth patterns. (A) Plot of the penetration depth as a function of incident laser angle for a glass–media interface. Penetration depth is defined as the location where field intensity drops e^{-2}, or 87%, from that at the surface. The dashed line indicates a penetration depth of 1 μm occurring at $\theta_{i2} = \theta_C + 0.074°$, and the geometry of *S. elongatus* is shown in the inset for reference. (B) Surface plot of evanescent field, 1 μm from the surface, with power intensity plotted to indicate the photoinhibited, growth, and negligible-growth regions, based on thresholds measured for radiant light. Based on these values an elliptical ring pattern of growth is predicted, as shown by the useful portion of the power spectrum shown in green shading (region 2). The vertical line plot indicates the useful light intensity decay with distance.

the dashed line indicates a penetration depth of 1 μm which occurs at an angle of incidence of $\theta_{i2} = \theta_C + 0.074°$. As shown, the penetration depth of the evanescent field is a strong function of incident angle, with values corresponding to the inherent lengthscale of the bacterium occurring only near the critical angle (below 0.5° past critical). Because of this narrow envelope, only cells settling onto the surface will be within the range of the evanescent field. While the extent of the evanescent field and the size of the bacterium are well established (as shown together in Fig. 4), the method does not enable resolution on the scale of individual thylakoid membranes to determine the interaction between the evanescent field and specific photocenters within the cell. Growth of cells is instead attributed to excitation of photocenters assumed to be distributed around

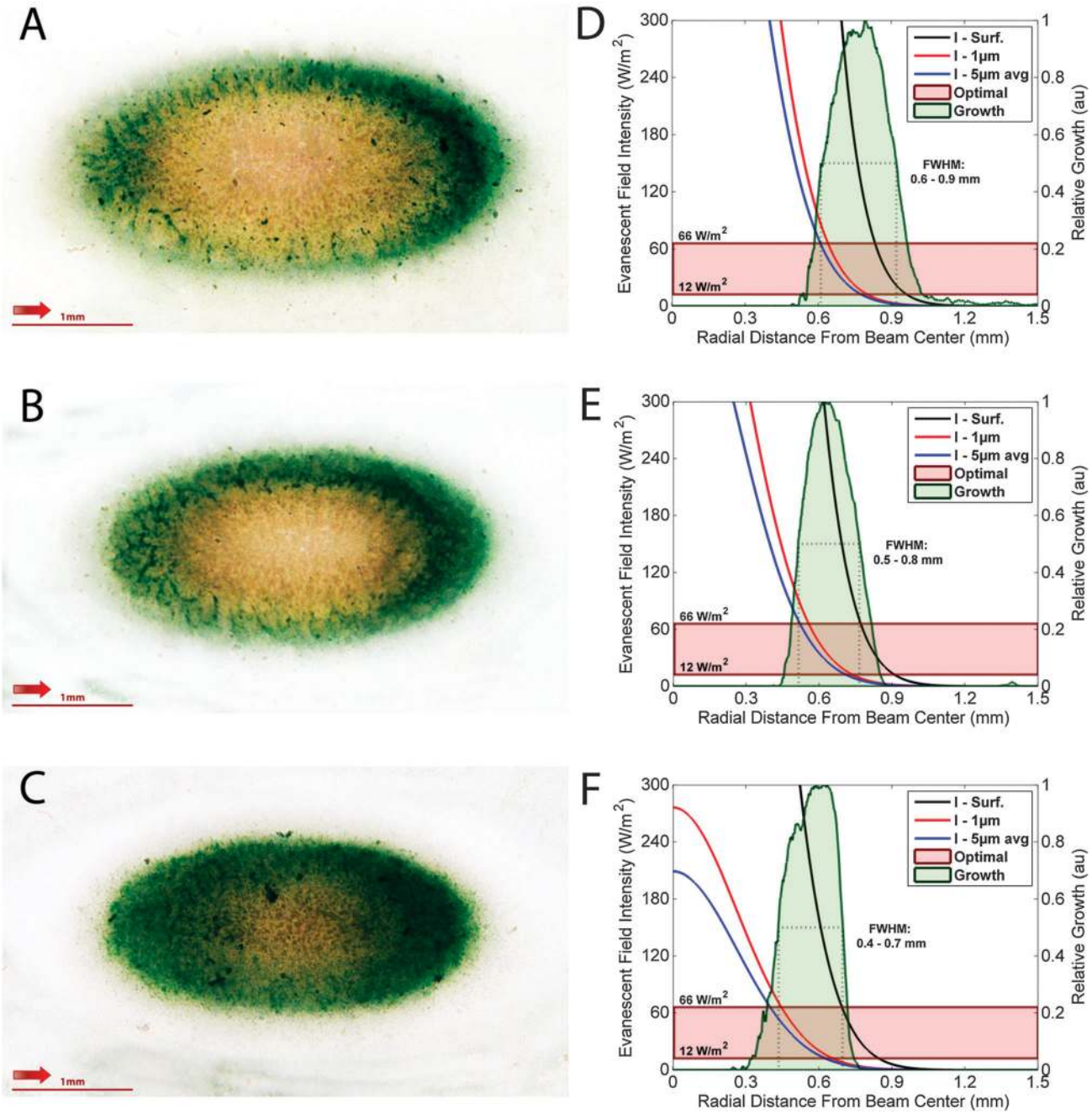

Fig. 5 Growing photosynthetic bacteria using *evanescent light*. (A–C) Images of cyanobacteria growth patterns resulting from evanescent excitation at the glass–media interface for incident light powers of 1 mW, 0.5 mW, and 0.25 mW, respectively. The elliptical growth patterns correspond to the evanescent field geometry, and show distinct regions of photobleaching (centre), and growth, surrounded by negligible growth. (D–F) Corresponding growth profiles for each light power with the corresponding evanescent field intensities plotted at the surface, 1 μm above the surface, and as a 5 μm average. The power range determined from the direct radiation experiments (Fig. 2) is shown by the red band for reference. The full-width at half maximum indicating growth onset is observed at 1 μm intensity levels of 79 ± 10 W m^{-2}, and observed at 60 ± 8 W m^{-2} for the 5 μm average light intensity. These values bracket the 66 W m^{-2} threshold determined for radiant light at this wavelength.

the cell where the average evanescent intensity across the cell dimension falls within the range of acceptable intensities.

Fig. 4B shows the predicted evanescent field intensity in the plane, and the characteristic oval shape for an incident 0.5 mm diameter Gaussian beam at $\lambda = 633$ nm. The intensity values indicated correspond to the evanescent light intensity at 1 μm from the glass–media interface, with an incident angle of 62° ($\theta_{i2} = \theta_C + 0.5°$) and a penetration depth of 400 nm. Based on the above-determined threshold light intensity for the red light employed here (66 W m^{-2}, at 633 nm), the expected growth regions can be predicted based on the calculated evanescent field intensity. As shown in Fig. 4B, in region 1 the evanescent field intensity exceeds this threshold and would be expected to lead to photoinhibition in a radiant light system. This analysis would predict an elliptical ring pattern of growth, as shown by the useful portion of the power spectrum shown in green shading (region 2). The vertical line plot indicates the useful light intensity decay with distance. Relatively intense growth is expected near the inside boundary where useful light intensities are high, and growth rates would decay with the light intensity outward. Although the sharpness of the inside edge of the growth profile is an artefact of the threshold boundary conditions, the model provides the predicted pattern of growth for a photosynthetic microorganism cultured in this evanescent field.

Evanescent light based excitation of the culture was performed using the experimental setup shown in Fig. 1B. Three laser powers were employed (1 mW, 0.5 mW, 0.25 mW) with incident laser angles of 62° ($\theta_{i2} = \theta_C + 0.5°$), and total internal reflection was ensured by measuring the output intensity. Each experiment was performed in triplicate and the cultures were exposed to the evanescent field for 72 hours. Fig. 5A–C show substantial bacteria growth in response to the evanescent light field at the surface of the glass–media interface. The growth patterns showed the elliptical shape mirroring the evanescent light field intensity, and delineate the three characteristic regions (photoinhibition, growth, negligible-growth), providing data on the onset of growth under evanescent light. As the laser power was reduced (Fig. 5A–C) the radial distribution moved inward, consistent with the change in the light intensity profile. To relate the observed growth to the evanescent field intensity, the images were filtered for green intensity, scaled along the axis of the beam, and integrated to provide growth profiles. Fig. 5D–F shows the growth profiles for each light power with the corresponding evanescent field intensities plotted at the surface, 1 μm above the surface, and as a 5 μm average. Due to rapidly decaying nature of the evanescent field, the surface intensity is much higher than that at 1 μm above the surface, which is also similar to the average intensity over the first 5 μm (both 1 μm and 5 μm are relevant lengthscales of this rod-shaped bacteria). The power range determined from the direct radiation experiments is shown by the red band for reference. The onset of growth occurs at a radial location where the evanescent light intensity—as measured at 1 μm and as a 5 μm average—drops to a value corresponding to the threshold of 66 W m^{-2}, established from direct radiation experiments. As the total intensity of light is decreased (Fig. 5A–F) the location of the onset intensity moves inward, and remains consistent with the predicted power curves. Specifically, the full-width at half maximum indicating growth onset is observed at 1 μm intensity levels of 79 ± 10 W m^{-2}, and observed at 60 ± 8 W m^{-2} for the 5 μm average light intensity. Importantly, these results both demonstrate growth of photosynthetic bacteria using evanescent light, and provide metrics for their successful cultivation within this unique light field.

The growth patterns shown in Fig. 5, and additional experiments (Fig. S2, ESI†), show some downbeam bias, that is, growth intensity increases with distance from the laser source. When the cells interact with the evanescent field near the surface, some of the light is absorbed and utilized, while some of the light is scattered. The light will be scattered preferentially in the direction of the beam.[29] With the present experimental setup, this scattered light would contribute to higher growth rates, and thicker biofilms, on the downbeam side of the ring pattern. This effect was noticed in most cases with downbeam growth biases of 1%, 8% and 15% for the 0.25 mW, 0.50 mW, 1.0 mW cases plotted in Fig. 5. Although the extent of this bias varied between trials, and some trials showed negligible, and even a small upbeam bias (details in Fig. S3, ESI†), the effect was in general small and in all cases less than 15%. While it is likely that downbeam bias and secondary scattering effects influence growth, the relative symmetry of the growth patterns indicates that the downbeam scattering effect is minor.

The additional effect of light penetration depth was investigated using incident light at larger angles past critical ($\theta_C < \theta_{i2} < \theta_C + 5°$). At angles greater than 0.5° over critical (as plotted in Fig. 5), however, only faint growth rings were observed. We attribute the lack of growth at larger angles to the change in penetration depth which diminishes rapidly with increasing incident angle, as shown in Fig. 4A. Specifically, the penetration depth corresponds to the minor-dimension of the rod-shaped bacterium (1 μm) only at angles less than $\theta_C + 0.074°$. These results are thus consistent with the observed evanescent growth patterns in that the penetration depth approached the cell diameter only at small angles away from critical.

4. Conclusion

We have demonstrated that evanescent fields can be utilised to grow photosynthetic bacteria. Cultures of *S. elongatus* were exposed to direct laser illumination ($\lambda = 633$ nm) and grew optimally with light intensities that ranged from 12 to 66 W m^{-2}. When excited with an evanescent field, this optimal growth band occurred between surface intensities of 30–650 W m^{-2}. This difference was attributed to the exponential decay of evanescent fields into the culture media, and at heights of 1–5 μm from the surface, approximately the width of an individual cell, the intensity falls within the 3–60 W m^{-2} ideal. This narrowly confined region for growth enables targeted light delivery to individual bacteria by tapping energy from the evanescent field. This work provides an alternative to current practices of delivering radiant light to cultures of photosynthetic bacteria. While direct illumination of a thin biofilm of cells may also be a viable approach to achieve controlled illumination, it presents no significant advantage over direct illumination of a bulk culture. In contrast the confinement inherent to the evanescent approach enables select illumination

of surface cells and improved control, particularly in regards to the spatial distribution of light. Furthermore, the cell-scale limited extent of the light field provides a tool to probe microorganism response which is not possible with direct illumination of thin microbial biofilms and provides a platform for improved understanding of photosynthetic processes in microorganisms.

Acknowledgements

The authors wish to gratefully acknowledge funding from the Natural Science and Engineering Research Council of Canada (NSERC) through a Strategic Projects Grant to DS in partnership with Canadian Bioenergy Corp, and infrastructure funding from the Canada Foundation for Innovation (CFI). Seed funding from the Atkinson Center for a Sustainable Future at Cornell University is also gratefully acknowledged. Scholarships from NSERC and the Pacific Institute for Climate Solutions for M.D.O. are gratefully acknowledged, as are helpful discussions with Dr Francis Nano's research group (University of Victoria), Dr Lars Angenent (Cornell University) and ongoing collaboration with Dr Vincent Martin (Concordia University).

References

1 Govindjee and D. Shevela, *Front. Plant Physiol.*, 2011, **2**, 28.
2 J. Bender and P. Phillips, *Bioresour. Technol.*, 2004, **94**, 229–238.
3 P. Spolaore, C. Joannis-Cassan, E. Duran and A. Isambert, *J. Biosci. Bioeng.*, 2006, **101**, 87–96.
4 K. Yamaguchi, *J. Appl. Phycol.*, 1996, **8**, 487–502.
5 N. K. Singh and D. W. Dhar, *Agron. Sustainable Dev.*, 2011, **31**, 605–629.
6 D. E. Robertson, S. A. Jacobson, F. Morgan, D. Berry, G. M. Church and N. B. Afeyan, *Photosynth. Res.*, 2011, **107**, 269–277.
7 A. Melis, *Energy Environ. Sci.*, 2012, **5**, 5531–5539.
8 A. A. Boghossian, M.-H. Ham, J. H. Choi and M. S. Strano, *Energy Environ. Sci.*, 2011, **4**, 3834–3843.
9 Y. K. Lee, *J. Appl. Phycol.*, 2001, **13**, 307–315.
10 C. U. Ugwu, H. Aoyagi and H. Uchiyama, *Bioresour. Technol.*, 2008, **99**, 4021–4028.
11 Y.-K. Lee, *Trends Biotechnol.*, 1986, **4**, 186–189.
12 D. Briassoulis, P. Panagakis, M. Chionidis, D. Tzenos, A. Lalos, C. Tsinos, K. Berberidis and A. Jacobsen, *Bioresour. Technol.*, 2010, **101**, 6768–6777.
13 C.-F. Ji, J. Legrand, J. Pruvost, Z.-A. Chen and W. Zhang, *Int. J. Hydrogen Energy*, 2010, **35**, 7200–7205.
14 K. Issarapayup, S. Powtongsook and P. Pavasant, *J. Biotechnol.*, 2009, **142**, 227–232.
15 C.-Y. Chen, G. D. Saratale, C.-M. Lee, P.-C. Chen and J.-S. Chang, *Int. J. Hydrogen Energy*, 2008, **33**, 6886–6895.
16 J.-W. Zijffers, M. Janssen, J. Tramper and R. Wijffels, *Mar. Biotechnol.*, 2008, **10**, 404–415.
17 J. C. Ogbonna, T. Soejima and H. Tanaka, *J. Biotechnol.*, 1999, **70**, 289–297.
18 D. Dye, J. Muhs, B. Wood and R. Sims, *J. Sol. Energy Eng. Trans.-ASME*, 2011, **133**, 015001–015007.
19 S. Cookson, N. Ostroff, W. L. Pang, D. Volfson and J. Hasty, *Mol. Syst. Biol.*, 2005, DOI: 10.1038/msb4100032.
20 A. C. Rowat, J. C. Bird, J. J. Agresti, O. J. Rando and D. A. Weitz, *Proc. Natl. Acad. Sci. U. S. A.*, 2009, **106**, 18149–18154.
21 G. B. Salieb-Beugelaar, G. Simone, A. Arora, A. Philippi and A. Manz, *Anal. Chem.*, 2010, **82**, 4848–4864.
22 P. Shah, I. Vedarethinam, D. Kwasny, L. Andresen, M. Dimaki, S. r. Skov and W. E. Svendsen, *Sens. Actuators, B*, 2011, **156**, 1002–1008.
23 P. Sun, *Biosens. Bioelectron.*, 2011, **26**, 1993–1999.
24 Y. Asato, *Cell. Mol. Life Sci.*, 2003, **60**, 663–687.
25 R. J. Ritchie, D. A. Trautman and A. W. D. Larkum, *Plant Cell Physiol.*, 1997, **38**, 1232–1241.
26 A. K. Clarke, D. Campbell, P. Gustafsson and G. Oquist, *Planta*, 1995, **197**, 553–562.
27 S. Bhattacharya, A. Datta, J. M. Berg and S. Gangopadhyay, *J. Microelectromech. Syst.*, 2005, **14**, 590–597.
28 D. Axelrod, T. P. Burghardt and N. L. Thompson, *Annu. Rev. Biophys. Bioeng.*, 1984, **13**, 247–268.
29 D. Axelrod, in *Biophysical Tools for Biologists, Vol 2: In Vivo Techniques*, Elsevier Academic Press Inc, San Diego, 2008, vol. 89, pp. 169–221.
30 CIE, *Colorimetry—technical report 15*, Commission Internationale de l'Eclairage, Vienna, 2004.
31 J. N. Lohscheider, M. Strittmatter, H. Küpper and I. Adamska, *PLoS One*, 2011, **6**, e20134.
32 R. Capentier, *Handbook of photosynthesis*, CRC Press, 2005, ch. 19.
33 R. D. Kulkarni and S. S. Golden, *J. Bacteriol.*, 1994, **176**, 959.
34 T. D. B. MacKenzie, R. A. Burns and D. A. Campbell, *Plant Physiol.*, 2004, **136**, 3301–3312.
35 H. Rai, *Hydrobiologia*, 1995, **308**, 51–59.
36 R. Kaňa, O. Prášil, O. Komárek, G. C. Papageorgiou and Govindjee, *Biochim. Biophys. Acta,Bioenerg.*, 2009, **1787**, 1170–1178.
37 A. V. Ruban, M. P. Johnson and C. D. P. Duffy, *Energy Environ. Sci.*, 2011, **4**, 1643–1650.